Molecular Pharmacology Fast Forward. Published on October 1, 2021 as DOI: 10.1124/molpharm.121.000345
This article has not been copyedited and formatted. The final version may differ from this version.

Identification of Key Amino Acids that Impact Organic Solute Transporter Alpha/Beta (OSTα/β)

Authors

William A. Murphy[*], James J. Beaudoin[*], Tuomo Laitinen, Noora Sjöstedt, Melina M. Malinen, Henry Ho, Peter W. Swaan, Paavo Honkakoski[#], Kim L.R. Brouwer[#]

[*]Contributed equally to this work

ORCiD Numbers

William A. Murphy (0000-0002-7476-9248)

James J. Beaudoin (0000-0002-6926-8844)

Tuomo Laitinen (0000-0003-1539-2142)

Noora Sjöstedt (0000-0001-6960-7757)

Melina M. Malinen (0000-0002-9955-5043)

Henry Ho (0000-0003-1138-9149)

Peter W. Swaan (0000-0003-1767-1487)

Paavo Honkakoski (0000-0002-4332-3577)

Kim L.R. Brouwer (0000-0003-1945-4929)

Molecular Pharmacology Fast Forward. Published on October 1, 2021 as DOI: 10.1124/molpharm.121.000345
This article has not been copyedited and formatted. The final version may differ from this version.

Affiliations

Division of Pharmacotherapy and Experimental Therapeutics, UNC Eshelman School of Pharmacy, University of North Carolina, Chapel Hill, North Carolina (W.A.M., J.J.B., N.S., M.M.M., H.H., P.H., K.L.R.B.)

Department of Pharmaceutical Sciences, University of Maryland, Baltimore, Maryland (P.W.S.)

School of Pharmacy, University of Eastern Finland, Kuopio, Finland (T.L., M.M.M., P.H.)

Current Affiliation

Dr. Noora Sjöstedt. *Address*: Division of Pharmaceutical Biosciences, Faculty of Pharmacy, University of Helsinki, Helsinki, Finland.

Dr. Melina Malinen. *Address*: Orion Corporation, Orion Pharma, Espoo, Finland.

Molecular Pharmacology Fast Forward. Published on October 1, 2021 as DOI: 10.1124/molpharm.121.000345
This article has not been copyedited and formatted. The final version may differ from this version.

Running Title: *Key Amino Acids that Impact OSTα/β*

#Corresponding Authors:

Dr. Kim L.R. Brouwer. *Address*: Division of Pharmacotherapy and Experimental Therapeutics, UNC Eshelman School of Pharmacy, University of North Carolina at Chapel Hill, CB #7569 Kerr Hall, Chapel Hill, NC 27599-7569. *Telephone*: (919) 962-7030. *Fax*: (919) 962-0644. *E-mail*: kbrouwer@unc.edu.

Dr. Paavo Honkakoski. *Address*: School of Pharmacy, University of Eastern Finland, FI-70219 Kuopio, Finland. *Telephone*: +358 40 355 2490. *E-mail*: paavo.honkakoski@uef.fi.

Number of text pages: 32

Number of tables: 0

Number of figures: 5

Number of references: 50

Number of words in *Abstract*: 250

Number of words in *Introduction*: 664

Number of words in *Discussion*: 1,426

Abbreviations

Alanine (Ala; A); Asparagine (Asn; N); Cystine (Cys; C); Glutamate (Glu; E); Glutamine (Gln; Q); Lysine (Lys; K); Phenylalanine (Phe; F); Serine (Ser; S); Threonine (Thr; T)

ASBT, apical sodium-dependent bile acid transporter; DAPI, 4′,6-diamidino-2-phenylindole; ECF, extracellular fluid; FXR, farnesoid X receptor; GCA, glycocholate; HRP, horseradish

Molecular Pharmacology Fast Forward. Published on October 1, 2021 as DOI: 10.1124/molpharm.121.000345
This article has not been copyedited and formatted. The final version may differ from this version.

peroxidase; MOPS, 4-morpholinepropanesulfonic acid; OSTα/β, organic solute transporter alpha/beta; PBS, phosphate-buffered saline; PCR, polymerase chain reaction; sec, second; TCA, taurocholate; TBST, Tris-buffered saline with Tween 20; TMD, transmembrane domain; WT, wild-type

Molecular Pharmacology Fast Forward. Published on October 1, 2021 as DOI: 10.1124/molpharm.121.000345
This article has not been copyedited and formatted. The final version may differ from this version.

Abstract

Organic solute transporter alpha/beta (OSTα/β; SLC51A/B) is a bidirectional bile acid transporter localized on the basolateral membrane of hepatic, intestinal, and renal epithelial cells. OSTα/β plays a critical role in intestinal bile acid reabsorption and is upregulated in hepatic diseases characterized by elevated bile acids, while genetic variants in *SLC51A/B* have been associated with clinical cholestasis. OSTα/β also transports and is inhibited by commonly used medications. However, there is currently no high-resolution structure of OSTα/β, and structure-function data for OSTα, the proposed substrate-binding subunit, are lacking. The present study addressed this knowledge gap and identified amino acids in OSTα that are important for bile acid transport. This was accomplished using computational modeling and site-directed mutagenesis of the OSTα subunit to generate OSTα/β mutant cell lines. Out of the ten OSTα/β mutants investigated, four (S228K, T229S, Q269E, Q269K) exhibited decreased [^{3}H]-taurocholate (TCA) uptake (ratio of geometric means relative to OSTα/β WT of 0.76, 0.75, 0.79, 0.13, respectively). Three OSTα/β mutants (S228K, Q269K, E305A) had reduced [^{3}H]-TCA efflux % (ratio of geometric means relative to OSTα/β WT of 0.86, 0.65, 0.79, respectively). Additionally, several OSTα/β mutants demonstrated altered expression and cellular localization when compared to OSTα/β WT. In summary, we identified OSTα residues (Ser228, Thr229, Gln269, Glu305) in predicted transmembrane domains that affect expression of OSTα/β and may influence OSTα/β-mediated bile acid transport. These data advance our understanding of OSTα/β structure/function and can inform future studies designed to gain further insight into OSTα/β structure, or to identify additional OSTα/β substrates and inhibitors.

Molecular Pharmacology Fast Forward. Published on October 1, 2021 as DOI: 10.1124/molpharm.121.000345
This article has not been copyedited and formatted. The final version may differ from this version.

Significance Statement

OSTα/β is a clinically important transporter involved in enterohepatic bile acid recycling with currently no high-resolution protein structure and limited structure-function data. This study identified four OSTα amino acids (Ser228, Thr229, Gln269, Glu305) that affect expression of OSTα/β and may influence OSTα/β-mediated bile acid transport. These data can be utilized to inform future investigation of OSTα/β structure and refine molecular modeling approaches to facilitate the identification of substrates and/or inhibitors of OSTα/β.

Molecular Pharmacology Fast Forward. Published on October 1, 2021 as DOI: 10.1124/molpharm.121.000345
This article has not been copyedited and formatted. The final version may differ from this version.

Introduction

The importance of the organic solute transporter alpha/beta (OSTα/β; SLC51A/B) in human physiology and disease is growing in recognition as critical roles for this protein in the transport of bile acids have emerged (Beaudoin et al., 2020a). This bidirectional, heteromeric transport protein is expressed predominantly on the basolateral membrane of intestinal, renal, biliary, and hepatic epithelial cells (Ballatori, 2005; Uhlen et al., 2015). While its expression is low in the healthy human liver (Uhlen et al., 2015), OSTα/β protein is significantly upregulated in hepatic diseases associated with altered bile acid homeostasis (*i.e.*, primary biliary cholangitis and nonalcoholic steatohepatitis) (Boyer et al., 2006; Malinen et al., 2018). Disease-associated upregulation of hepatic OSTα/β may facilitate basolateral bile acid efflux into sinusoidal blood, thereby protecting hepatocytes from damage due to accumulating toxic bile acids (Boyer et al., 2006; Chai et al., 2015; Malinen et al., 2018). This hypothesis is supported by the finding that OSTα/β is inhibited by some xenobiotics associated with cholestatic hepatotoxicity (*e.g.*, troglitazone sulfate, ethinyl estradiol). Also, OSTα/β preferentially transports conjugates of relatively hydrophobic, hepatotoxic bile acids such as tauro- and glycochenodeoxycholate compared to more hydrophilic bile acids including taurocholate (TCA) and glycocholate (GCA) (Beaudoin et al., 2020b; Suga et al., 2019). Furthermore, OSTα/β expression is tightly regulated by farnesoid X receptor (FXR), a nuclear receptor activated during hepatocellular bile acid accumulation.

OSTα/β plays an important role in the enterohepatic circulation of bile acids under non-cholestatic conditions; bile acids in the intestinal lumen are transported into enterocytes by the apical sodium-dependent bile acid transporter (ASBT) and undergo efflux into the mesenteric circulation by OSTα/β (Dawson et al., 2005). Case studies in three pediatric patients suffering

Molecular Pharmacology Fast Forward. Published on October 1, 2021 as DOI: 10.1124/molpharm.121.000345
This article has not been copyedited and formatted. The final version may differ from this version.

from cholestasis, congenital diarrhea, and elevated liver transaminases highlight the importance of OSTα/β in hepatobiliary bile acid homeostasis. These patients had rare genetic mutations in *SLC51A* (c.556C>T, p.Q186stop) (Gao et al., 2019) and *SLC51B* (c.79delT, p.F27frameshift) (Sultan et al., 2018) resulting in truncated OSTα and OSTβ protein, respectively. Impaired OSTα/β function in hepatocytes, enterocytes, and cholangiocytes likely results in cellular accumulation of bile acids and could explain these clinical phenotypes (Sultan et al., 2018). OSTα/β also transports endogenous steroid hormones and several drugs including digoxin, docetaxel, statins, and sulfasalazine (Schwarz, 2012; Seward et al., 2003; Wang et al., 2001). However, the true contribution of this transporter to drug disposition and toxicity in health and disease is unknown and commonly unaccounted for in predictive models utilized during drug development. A better understanding of OSTα/β protein structure and function is needed to inform future studies and facilitate accurate predictions of the role of this transporter in drug disposition and drug interactions in healthy and diseased populations.

Twenty years after the initial discovery of this transporter in a hepatic cDNA screen (Wang et al., 2001), OSTα/β still lacks a high-resolution 3D structure. Alternative strategies to obtain information on protein structure include evolutionary conservation analysis, prediction of topology, homology modeling, and molecular modeling. Homology-based modeling, in tandem with three-dimensional molecular modeling is a common approach to elucidate protein-substrate interactions and identify key amino acids required for substrate recognition and transport (Schlessinger et al., 2018). The MEMSAT-SVM is a sequence-based platform that predicts pore-lining helices in transmembrane proteins that are essential for substrate interaction (Nugent and Jones, 2012) and can be utilized to guide *in vitro* functional studies. Previous *in vitro* work revealed that OSTα is likely the substrate-binding subunit, while co-expression of OSTβ on the

Molecular Pharmacology Fast Forward. Published on October 1, 2021 as DOI: 10.1124/molpharm.121.000345
This article has not been copyedited and formatted. The final version may differ from this version.

plasma membrane is required for transport function (Seward et al., 2003). However, more data on OSTα/β structure-function pertaining to bile acid transport is needed. Site-directed mutagenesis, informed by computational modeling, offers an attractive opportunity to study the relative contributions of individual amino acids to OSTα/β structure and function. This approach has been used previously for other human transporters (Gruetz et al., 2016; Scalise et al., 2018; Zou et al., 2018). The present study employed *in silico* computational tools, *in vitro* site-directed mutagenesis, and *in vitro* functional assays to identify amino acids in OSTα that influence bile acid transport.

Molecular Pharmacology Fast Forward. Published on October 1, 2021 as DOI: 10.1124/molpharm.121.000345
This article has not been copyedited and formatted. The final version may differ from this version.

Materials and Methods

Chemicals and Reagents. Unlabeled TCA and GCA were purchased from Chem-Impex International (Wood Dale, IL) and Sigma-Aldrich (St. Louis, MO), respectively. [^{3}H]-TCA (6.50–9.74 Ci/mmol, radiochemical purity >97%) and [^{14}C]-GCA, sodium salt (51.58 mCi/mmol, radiochemical purity >97%) were obtained from PerkinElmer Life Sciences (Boston, MA). Gibco™ Dulbecco's Modified Eagle Medium (catalog no. 11960-044), PureLink™ HiPure Plasmid Miniprep Kit, Corning® BioCoat™ 24-well plates (catalog no. 08774124), radioimmunoprecipitation assay lysis and extraction buffer (catalog no. 89900), Pierce™ dithiothreitol extraction buffer (catalog no. 20291), Pierce™ bicinchoninic acid protein assay kit, NuPAGE™ LDS Sample Buffer (catalog no. NP0007), NuPAGE 4-12% Bis-Tris gel (catalog no. NP0322Box), NuPAGE MOPS SDS Running Buffer (catalog no. NP001), NuPAGE Transfer Buffer (catalog no. NP0006), Restore™ Western Blot Stripping Buffer (catalog no. 21063), LabTek® Chamber Slides (catalog no. 177445), fetal bovine serum, L-glutamine, penicillin-streptomycin, and goat-anti-mouse IgG AlexaFluor™ 488 secondary antibody (catalog no. A11001) were all purchased from Thermo Fisher Scientific (Waltham, MA). cOmplete™ ULTRA Tablets, Mini, EDTA-free, *EASY*pack Protease Inhibitor Cocktail (catalog no. 05892791001), PhosSTOP™ (catalog no. 04906845001), rabbit-anti-OSTβ antibody (catalog no. HPA008533), mouse-anti-β-actin antibody (catalog no. A1978), and 4′,6-diamidino-2-phenylindole (DAPI) (catalog no. D9542) were purchased from Sigma-Aldrich, and rabbit-anti-OSTα antibody (catalog no. ab103442) from Abcam (Cambridge, MA). The OSTα antibody used for Western blot and immunocytochemistry analysis (ab103442) was a polyclonal mixture with an immunogen corresponding to a region within human OSTα C-terminal amino acids (305-335). Horseradish peroxidase (HRP)-conjugated anti-rabbit antibody and HRP-conjugated anti-

Molecular Pharmacology Fast Forward. Published on October 1, 2021 as DOI: 10.1124/molpharm.121.000345
This article has not been copyedited and formatted. The final version may differ from this version.

mouse antibody were obtained from Jackson ImmunoResearch (West Grove, PA), and Fluoromount-G™ Mounting Medium (catalog no. 0100-01) and 10% normal goat serum from Southern Biotech (Birmingham, AL). The Q5® Site-Directed Mutagenesis Kit was obtained from New England Biolabs (Rowley, MA)

Identification of OSTα amino acids for mutagenesis. Two approaches were used to select specific OSTα amino acids for mutation studies (Fig. 1). The first approach involved evolutionary conservation and topology prediction tools. Evolutionary conservation of amino acids in human OSTα (UniProtKB protein identifier: Q86UW1) was evaluated using OSTα protein sequences from mouse (Q8R000), rat (D4AC81), bovine (Q3T124), and skate (Q90YM5). In addition, several topology prediction tools (TOPCONS (Tsirigos et al., 2015), CCTOP (Dobson et al., 2015), DAS (Cserzö et al., 1997), PRED-TMR2 (Pasquier et al., 1999), HMMTOP (Tusnády and Simon, 2001), TMHMM (Krogh et al., 2001), SOSUI (Hirokawa et al., 1998) and MEMSAT-SVM (Nugent and Jones, 2012) were used to predict which OSTα amino acids belong to the transmembrane domains (TMDs). The majority of these tools predicted a total of seven TMDs in OSTα, and at least five TMDs were unanimously predicted. MEMSAT-SVM was used to predict which of the TMDs form the pore-lining region of OSTα. Evolutionarily conserved, hydrophilic amino acids (Ser228, Thr229, Gln260, Gln269) in those TMDs were selected for mutagenesis (Fig. 2) in order to study their individual impact on transport function. A number of non-conservative and relatively conservative amino acid substitutions (Bordo and Argos, 1991) were used to generate the following mutants of OSTα: S228K, S228T, T229S, Q260K, Q269E, and Q269K.

The second approach involved homology-based models. Since the protein structure of OSTα/β is unavailable, the models were constructed based on the assumption that the transmembrane

Molecular Pharmacology Fast Forward. Published on October 1, 2021 as DOI: 10.1124/molpharm.121.000345
This article has not been copyedited and formatted. The final version may differ from this version.

helical parts of the OSTα protein are closely related from a structural standpoint to selected transporter templates even if the exact sequence homology is low. OsSweet, a sugar transporter and a homolog of the human SLC50A1 (Tao et al., 2015), was selected as the template due to its similar seven TMD topology to OSTα and the lack of an available seven TMD eukaryotic SLC template. In addition to their similar topology, the OsSweet folding conformation (inside open) is consistent with the physiological function of OSTα/β to transport bile acids out of hepatocytes (efflux phase) (Dawson et al., 2010; Guo et al., 2018). Tools such as ClustalW (Larkin et al., 2007), PROMALS3D (Pei et al., 2008), and T-COFFEE (Notredame et al., 2000) were not able to provide reasonable alignments of predicted TMDs. However, locations of the transmembrane helices were successfully predicted with TMHMM (Krogh et al., 2001), TMpred (Ikeda et al., 2003), and DAS (Cserzö et al., 1997). Aligned human, mouse, bovine, and rat OSTα sequences were used for the final TMD prediction. Homology models were constructed based on a manually optimized alignment of transmembrane helices using the standard settings of Discovery Studio (BIOVIA, Dassault Systèmes, San Diego, CA, 2020) from the OsSweet template (PDB: 5CTH) with an inward-open structure that included a co-crystallized additive polyethylene glycol 400 (Supplemental Fig. 1A). The single OSTβ transmembrane helix was modeled based on helix-helix interactions between subunits of the trimeric OsSweet structure (Supplemental Fig. 1B). Prior to docking studies, the homology models from Discovery Studio were pre-processed and minimized using the Schrödinger Suite 2020-1 protein preparation wizard tool with modules Epik, Impact and Prime (Schrödinger, LLC, New York, NY, 2020). Structure of the TCA substrate was parametrized and minimized using the Ligprep module (Schrödinger, LLC). Molecular docking studies were computed using the induced fit workflow of Schrödinger by employing the SP-setting for the Glide docking module, and side chain

Molecular Pharmacology Fast Forward. Published on October 1, 2021 as DOI: 10.1124/molpharm.121.000345
This article has not been copyedited and formatted. The final version may differ from this version.

movements of 5Å were considered for the conformational refinement using the Prime module. Based on the visualized OSTα amino acids and their mutual and substrate interactions, this approach led to the selection of four OSTα amino acids Cys103, Phe122, Asn298, Glu305 for alanine scanning mutagenesis (Morrison and Weiss, 2001). Finally, to qualitatively study the stability of the homology model of OSTα with a docked ligand (TCA) (Fig. 3), a molecular dynamics simulation was performed that included a phospholipid membrane model of 1,2-dimyristoyl-*sn*-glycero-3-phosphocholine, neutralized with ions and solvated with simple point-charge waters using Desmond (Maestro-Desmond Interoperability Tools, Schrödinger, LLC; Desmond Molecular Dynamics System, D. E. Shaw Research, New York, NY, 2021). The structure was first minimized using the protein preparation wizard of Schrodinger with a default heavy atom root-mean-square deviation constraint of 0.3 Å. The Desmond molecular dynamic simulation was unconstrained and run using orthorhombic periodic boundary conditions. In the simulation setup, the position of the membrane bilayer was first placed automatically on helices and the final orientation was adjusted manually. Prior to the molecular dynamics simulation, the system was subjected to a default relaxation protocol of Desmond and heated up to the simulation temperature. A 500-nanosecond simulation was run using the NPT protocol at 300 Kelvin temperature, pressure of 1.01325 bar, Noe-Hoover thermostat and a timestep of 2 femtoseconds. The OSTα/β model was inspected using a visualization program Visual Molecular Dynamics (VMD Version 1.9.3, NIH Center for Macromolecular Modeling and Bioinformatics, at the Beckman Institute, University of Illinois at Urbana-Champaign, Champaign, IL). Graphical illustrations were generated using PyMol (The PyMOL Molecular Graphics System, Version 2.0, Schrödinger, LLC).

Molecular Pharmacology Fast Forward. Published on October 1, 2021 as DOI: 10.1124/molpharm.121.000345
This article has not been copyedited and formatted. The final version may differ from this version.

DNA constructs and mutagenesis. Site-directed mutagenesis and the Flp-In™ cell and vector system were used to incorporate mutations into the OSTα subunit. A previously developed pcDNA5.1/FRT expression vector containing human wild-type (WT) *SLC51A* (NM_152672.5, OSTα) and *SLC51B* (NM_178859.3, OSTβ) (Malinen et al., 2018) was used as a template for mutagenesis using the Q5® Site-Directed Mutagenesis Kit, per the manufacturer's instructions. DNA primer pairs for the generation of each *SLC51A* mutant via polymerase chain reaction (PCR) (Supplemental Table 1) were obtained from Integrated DNA Technologies (Coralville, IA). Prior to ligation, the integrity of PCR products was evaluated by agarose gel electrophoresis. Subsequently, plasmids were transformed into high-efficiency New England Biolabs 5-alpha competent *E. coli* cells according to the manufacturer's instructions. Ampicillin-resistant colonies were isolated and expanded overnight in Luria-Bertani medium containing ampicillin (100 µg/mL) in an orbital shaker (37°C, 160 rpm). The PureLink™ HiPure Plasmid Miniprep Kit was used to isolate plasmids. The concentration and purity of DNA were measured using a NanoDrop spectrophotometer (model ND-1000, Thermo Fisher Scientific). The OSTα constructs were then confirmed by Sanger sequencing (Eurofins Genomics LLC, Louisville, KY).

Generation of OSTα/β WT and OSTα/β mutant overexpressing cell lines. Mock, OSTα/β WT, and OSTα/β mutant Flp-In™ 293 cell lines were generated using lipofection as described previously (Malinen et al., 2018). Established cell lines stably expressing WT OSTα and OSTβ are referred to hereafter as OSTα/β WT cells, and cell lines expressing mutated OSTα and WT OSTβ are referred to hereafter as OSTα/β mutants for which the OSTα amino acid substitution was specified (*e.g.*, S228K). Cells transfected with empty pcDNA5.1/FRT vector were referred to as Mock cells.

Molecular Pharmacology Fast Forward. Published on October 1, 2021 as DOI: 10.1124/molpharm.121.000345
This article has not been copyedited and formatted. The final version may differ from this version.

Cell culture/maintenance of Flp-In™ 293 cells. Mock, OSTα/β WT, and mutant cells were cultured at 37°C and 5% CO_2 in T-75 cell culture flasks (Sarstedt, Newton, NC) with Dulbecco's Modified Eagle Medium supplemented with 10% fetal bovine serum, 2 mM L-glutamine, and 100 U/mL penicillin-100 ug/mL streptomycin. Media was replaced every 3-4 days and cells were subcultured once weekly using 0.25% trypsin-EDTA for detachment. Passages 5-15 were used for all assays. Cell viability was determined by Trypan blue exclusion.

Uptake studies in Mock, OSTα/β WT, and mutant Flp-In™ 293 cells. The impact of the selected OSTα amino acid substitutions on OSTα/β-mediated uptake of [^{3}H]-TCA was assessed at 30 sec, a time point within the linear range of the initial uptake vs. time profile (Beaudoin et al., 2020b; Malinen et al., 2018). A concentration of 5 μM was selected to study TCA transport as it mimics the physiologic concentration of serum bile acids (4-5 μM) following a meal (Di Ciaula et al., 2017). Cells were seeded at a density of 5 x 10^5 cells/well on poly-D-lysine-coated Corning® BioCoat™ 24-well plates. Uptake studies were performed ~48 hr after seeding when cells had formed a confluent monolayer. Medium was aspirated and the cells were briefly washed twice with warm (37°C) sodium-free extracellular fluid (ECF) buffer (125 mM KCl, 25 mM $KHCO_3$, 0.4 mM K_2HPO_4, 10 mM D-glucose, 1.4 mM $CaCl_2$, 1.2 mM anhydrous $MgSO_4$ and 10 mM HEPES; pH 7.4), based on earlier OSTα/β uptake studies (Malinen et al., 2018; Malinen et al., 2019). Subsequently, cells were conditioned with 200 μL/well of 5 μM [^{3}H]-TCA or 5 μM [^{14}C]-GCA dosing solution in warm ECF buffer for 30 seconds (sec) in an incubator (37°C, 5% CO_2). Dosing solution was aspirated, and cells were briefly washed twice with ice-cold (4°C) ECF buffer. Each cell monolayer was solubilized with 400 μL of lysis buffer (0.5% Triton X-100 and 0.005% antifoam A in phosphate-buffered saline [PBS]) and the contents were mixed vigorously on a VWR VX-2500 Multi Tube Vortexer (Marshall Scientific, Hampton, NH)

Molecular Pharmacology Fast Forward. Published on October 1, 2021 as DOI: 10.1124/molpharm.121.000345
This article has not been copyedited and formatted. The final version may differ from this version.

for 20 min. To determine the amount of radiolabeled compound in cells, 300 µL aliquots of the cell lysate were added to 10 mL of BioSafe II counting cocktail (RPI, Mt. Prospect, IL) in scintillation vials. Radioactive counting was performed using a liquid scintillation analyzer (Tri-Carb 3100TR, PerkinElmer). Total cellular protein was determined by a Pierce™ bicinchoninic acid protein assay kit using an aliquot (25 µL) of cell lysate. Absorbances were read at 562 nm using a PowerWave XS microplate spectrophotometer (BioTek Instruments). Uptake assays were repeated on three separate days, with three technical replicates on each day, resulting in nine replicate samples for each cell line.

Efflux studies using Mock, OSTα/β WT, and mutant Flp-In™ 293 cells. Efflux studies were performed using the same methodology as described for uptake assays, except that the 30-sec substrate conditioning phase was extended to 10 min (preloading phase) to allow for maximal intracellular accumulation of substrate prior to efflux. A 10-min duration for the preload phase was selected to maximize intracellular [^{3}H]-TCA concentrations based on the finding that OSTα/β-mediated cellular uptake of [^{3}H]-TCA using the same Flp-In™ system plateaued at ~10 min (Malinen et al., 2018). The selected time point for the efflux phase was 5 min based on pilot studies. After this 10-min preloading phase, the dosing solution was aspirated, and cells were briefly washed twice with ice-cold ECF buffer. Efflux of preloaded substrate was initiated by incubating one row of wells with warm ECF buffer (200 µL/well). Plates were placed on a flat external plate warmer at 37°C for 5 min before transferring efflux buffer (*i.e.*, warm ECF buffer) from each well to a 96-deep well plate (Greiner Bio-One, Monroe, NC). Cell lysates after the 10-min preload were collected to evaluate total intracellular substrate content prior to efflux, while cell lysates after the subsequent 5-min efflux were collected separately to determine the residual intracellular substrate content. To determine the amount of radiolabeled compound in cells and

Molecular Pharmacology Fast Forward. Published on October 1, 2021 as DOI: 10.1124/molpharm.121.000345
This article has not been copyedited and formatted. The final version may differ from this version.

efflux buffer, 10 mL of BioSafe II counting cocktail was added to samples (300 µL aliquots of cell lysate or 200 µL of efflux buffer) in scintillation vials. Radioactive counting and measurement of total cellular protein for each cell line was performed as described above. Efflux assays were repeated on three separate days in triplicate samples on each day, resulting in nine replicate samples for each cell line. Efflux assays for homology-informed mutants (C103A, F122A, N298, E305A) were performed on separate occasions (*i.e.*, Group 2) from the other mutants (S228K, S228T, T229S, Q260K, Q269E, Q269K) designated as Group 1, using the same OSTα/β WT comparator cell line. Of note, one out of nine replicates for S228K, S228T, Q269E, and Q269K was lost due to a pipetting error.

Western blot analysis. Cells were detached with 5 mM EDTA at 37°C from the T-75 flasks. The resulting cell suspension (~7 x 10^6 cells) was centrifuged at 200*g* for 5 min. After removing the supernatant, 1 mL of Radioimmunoprecipitation assay Lysis and Extraction buffer, supplemented with cOmplete™ ULTRA Tablets, Mini, EDTA-free, *EASY*pack Protease Inhibitor Cocktail and PhosSTOP™, was mixed by vortex and whole cell lysates were collected. Total cellular protein for each cell line was quantified using a Pierce™ bicinchoninic acid protein assay kit. Lysate samples containing 20 µg of total protein were prepared for Western blot analysis in 10% (v/v) of 0.5M Pierce™ dithiothreitol extraction buffer and 25% (v/v) NuPAGE LDS Sample Buffer, and added to separate wells of a NuPAGE 4-12% Bis-Tris gel. After electrophoresis using NuPAGE MOPS SDS Running Buffer, proteins were transferred to a polyvinylidene difluoride membrane by incubating in NuPAGE Transfer Buffer overnight at 4°C. The membrane was blocked in a 5% milk solution for 1 hr before incubation with rabbit-anti-OSTα antibody (1:250 dilution) or rabbit-anti-OSTβ antibody (1:150 dilution) overnight at 4°C in 5% (w/v) bovine serum albumin/Tris-buffered saline with Tween 20 (TBST) buffer. To

Molecular Pharmacology Fast Forward. Published on October 1, 2021 as DOI: 10.1124/molpharm.121.000345
This article has not been copyedited and formatted. The final version may differ from this version.

establish a loading control, the membrane was incubated in mouse-anti-β-actin antibody (1:5,000 dilution) at room temperature in 5% bovine serum albumin/TBST for 1 hr. The membranes were washed with TBST three times and then incubated with HRP-conjugated anti-rabbit antibody (1:5,000 dilution) for OSTα and OSTβ, and HRP-conjugated anti-mouse antibody (1:10,000 dilution) for β-actin at room temperature in 5% milk/TBST for 1 hr. The imaging signal was produced using chemiluminescence reagents (ECL Select, GE Healthcare Bio-Sciences, Piscataway, NJ). Images were captured and processed using BioRad (ChemiDoc XRS+) imager and Image Lab software (Bio-Rad, Hercules, CA). OSTα and OSTβ were evaluated on the same membrane without stripping, while β-actin loading control was evaluated on the same membrane following stripping with Restore™ Western Blot Stripping Buffer for 15 min at room temperature (20°C).

Immunocytochemistry. Eight-well LabTek® Chamber Slides were coated using a 0.1 mg/mL poly-D-lysine solution. Mock, OSTα/β WT, and mutant cells were seeded at a density of $0.4x10^5$ cells/well. After growing to ~70% confluence, cells were fixed with 4% paraformaldehyde. Cells were permeabilized for 10 min with 200 µL of 0.5% saponin in PBS and then blocked with 150 µL of 10% normal goat serum in 0.1% saponin for 1 hr at room temperature. After removing the blocking solution, cells were incubated with either 150 µL of rabbit-anti-OSTα antibody (1:50 dilution) or rabbit-anti-OSTβ antibody (1:50 dilution) overnight at 4°C. Cells were washed with PBS three times and incubated with 150 µL of goat-anti-mouse IgG AlexaFluor™ 488 secondary antibody (1:200 dilution) for 1 hr at room temperature in the dark. Cells were then washed with PBS and Milli-Q® H_2O before incubating in 150 µL of a DAPI dilution (1:200) for 2 min at room temperature in the dark. Chamber walls were removed before adding 2-3 drops of Fluoromount-G™ Mounting Medium. A #1.5 glass coverslip (0.17mm) (VWR International,

Molecular Pharmacology Fast Forward. Published on October 1, 2021 as DOI: 10.1124/molpharm.121.000345
This article has not been copyedited and formatted. The final version may differ from this version.

Radnor, PA) was placed on top of chamber slides before storing at 4°C in the dark for ~24 hr to ensure hardening of the slide. Images were captured using a Nikon ECLIPSE Ti2 microscope (Nikon, Melville, NY) and optimized with Nikon NIS Elements software. All images were taken using a 60X oil immersion objective.

Data analysis. Uptake and efflux data for [^{3}H]-TCA and [^{14}C]-GCA were normalized to total cellular protein (pmol/mg of protein). OSTα/β WT and mutant cell uptake/efflux data were not adjusted for Mock cell function due to negligible (~5%) transport observed in Mock cells. No outliers were detected for uptake or efflux data using Grubbs's test. Percent (%) efflux was calculated by dividing the amount of radiolabeled substrate (pmol) per mg protein in ECF buffer following the 5-min efflux by the amount of radiolabeled substrate in cell lysate (pmol) per mg protein following the 10-min preload. Percent (%) of residual cellular substrate was calculated by dividing the amount of radiolabeled substrate in cell lysate (pmol) per mg protein following the 5-min efflux by the amount of radiolabeled substrate in cell lysate (pmol) per mg protein following the 10-min preload. The ratio of geometric mean uptake and % efflux for each mutant relative to OSTα/β WT, and corresponding 95% credible intervals, were calculated using a Bayesian generalized linear mixed model with group-specific terms. Experimental day was included as a random effect group-specific term for Bayesian models of uptake and efflux data. Group number was also included as a random effect group-specific term for the Bayesian model of efflux data (but not uptake data) since, as previously described, two groups of mutants were evaluated on separate occasions for efflux assays only. Protein expression data for OSTα/β WT and mutant cells were normalized to loading control (β-actin) and OSTα/β expression levels in Mock cells were subtracted from densitometry values from OSTα/β WT and each mutant cell line. ImageJ Version 1.53f 25 was used to normalize and quantify band intensity from Western

Molecular Pharmacology Fast Forward. Published on October 1, 2021 as DOI: 10.1124/molpharm.121.000345
This article has not been copyedited and formatted. The final version may differ from this version.

blots (Schneider et al., 2012). All statistical analyses were performed using R Version 1.4.1103 (R Core Team, 2020) and GraphPad Prism 9 (GraphPad Software, La Jolla, CA). Linear mixed analysis and Bayesian regression modeling were performed using the lme4 (Bates et al., 2015) and rstanarm (Goodrich et al., 2020) R packages, respectively (see Data Supplement 1).

Molecular Pharmacology Fast Forward. Published on October 1, 2021 as DOI: 10.1124/molpharm.121.000345
This article has not been copyedited and formatted. The final version may differ from this version.

Results

Molecular modeling. The 3D homology model studies indicated that despite the low similarity of residues, OSTα helices could be aligned reasonably well with those in the OsSweet template. In docking studies, most of the docking poses for TCA within the OSTα cavity were oriented so that the bile acid A-ring was pointing towards the extracellular space. This region of the substrate was consistently in close contact with amino acids Phe122 and Asn298 (Fig. 3). Notably, the corresponding residues in OsSweet were in contact with the respective ligand (Tao et al., 2015). The side chain of TCA was oriented towards the cytoplasm but was more flexible with fewer contacts with the surrounding helices due to the inward-open structure of the template (Fig. 3; Supplemental Fig. 2, Data Supplement 2 and 3). Of residues identified by evolutionary conservation and topology prediction, Thr229 and Gln269 were also oriented towards the predicted cavity of the homology model, Ser228 was facing the neighboring helix and Gln260 was placed away from the cavity (Fig. 3; Supplemental Fig. 2, Data Supplement 2 and 3). The final homology model appeared relatively stable over time, with helices showing the least fluctuation in 500 nanosecond simulations (Supplemental Fig. 3, Data Supplement 4).

OSTα/β-mediated Uptake. Out of ten mutants, four showed a decrease in [^{3}H]-TCA uptake (S228K, T229S, Q269E, Q269K) relative to OSTα/β WT. Specifically, the respective ratios of geometric mean 30-sec uptake relative to OSTα/β WT (95% credible interval) were 0.76 (0.67 – 0.88), 0.75 (0.65 – 0.86), 0.79 (0.68 – 0.90), and 0.13 (0.11 – 0.15) (Fig. 4).

OSTα/β-mediated Efflux. [^{3}H]-TCA % efflux (of the preloaded amount) was reduced in three mutant cells, S228K, Q269K and E305A, which showed respective ratios of the geometric mean efflux % relative to OSTα/β WT (95% credible interval) of 0.86 (0.78 – 0.95), 0.65 (0.59 – 0.71),

Molecular Pharmacology Fast Forward. Published on October 1, 2021 as DOI: 10.1124/molpharm.121.000345
This article has not been copyedited and formatted. The final version may differ from this version.

and 0.79 (0.72 – 0.87) (Fig. 4). These mutants also differed from OSTα/β WT in other transport parameters. Specifically, S228K and Q269K displayed increased % residual cellular [^{3}H]-TCA relative to OSTα/β WT (Supplemental Table 2). Due to similar [^{3}H]-TCA and [^{14}C]-GCA uptake/efflux data for Mock, OSTα/β WT, and mutant cell lines, [^{14}C]-GCA uptake/efflux was only studied for six mutants (S228K, S228T, T229S, Q260K, Q269E, Q269K) (*data not shown*).

OSTα and OSTβ Protein Levels. Protein levels of OSTα and OSTβ in Mock, OSTα/β WT, and mutant cells were assessed by densitometry of the Western blots (Supplemental Fig. 4). Mock cells, as expected, had negligible to low expression of both OSTα forms and OSTβ protein. The smaller OSTα immature precursor protein is believed to be localized to the endoplasmic reticulum while the mature OSTα glycoprotein is expressed on the plasma membrane (Dawson et al., 2005; Soroka et al., 2008). While OSTα/β WT cells had a low ratio of immature to mature OSTα proteins, three mutants (S228K, Q269E, Q269K) expressed higher absolute levels of immature OSTα than mature protein (Fig. 5a; Supplemental Fig. 4f). All mutant cells except Q260K had decreased OSTα mature and OSTβ protein expression compared to OSTα/β WT cells (Fig. 5; Supplemental Fig. 4). Mature OSTα expression had a strong correlation (r = 0.99) with expression of OSTβ protein for each mutant cell line relative to OSTα/β WT (Supplemental Fig. 4g).

OSTα and OSTβ cellular localization. Plasma membrane localization of OSTα and OSTβ was negligible in Mock cells. The localization of OSTα and OSTβ in mutant cell lines with altered [^{3}H]-TCA uptake and/or efflux (S228K, T229S, Q269E, Q269K, E305A) is shown in Fig. 5, while data for all mutant cells is presented in Supplemental Fig. 5. OSTα/β WT, C103A, and N298A cells had apparent plasma membrane localization of OSTα and OSTβ. Based on qualitative/visual inspection of the images (Supplemental Table 2), several mutant cells (F122A,

Molecular Pharmacology Fast Forward. Published on October 1, 2021 as DOI: 10.1124/molpharm.121.000345
This article has not been copyedited and formatted. The final version may differ from this version.

S228K, S228T, T229S, Q260K, Q269E, Q269K, E305A) appeared to have reduced plasma membrane expression of OSTα protein in comparison to OSTα/β WT. Five of these mutants (F122A, S228T, T229S, Q260K, E305A) also seemed to have increased intracellular localization of OSTα protein relative to OSTα/β WT. Two mutants (S228K, Q269K) showed negligible membrane localization of both OSTα and OSTβ protein. Interestingly, F122A, T229S, Q260K, and E305A cells all showed OSTβ plasma membrane staining similar to OSTα/β WT despite a reduction in OSTα membrane staining.

Molecular Pharmacology Fast Forward. Published on October 1, 2021 as DOI: 10.1124/molpharm.121.000345
This article has not been copyedited and formatted. The final version may differ from this version.

Discussion

OSTα/β is a clinically relevant transporter involved in enterohepatic recycling of bile acids, particularly in the small intestine, (Dawson et al., 2015; Gao et al., 2019; Sultan et al., 2018) and is upregulated in the human liver in certain diseases (Boyer et al., 2006; Malinen et al., 2018). Some drugs are substrates and/or inhibitors of OSTα/β (Beaudoin et al., 2020b; Malinen et al., 2019; Schwarz, 2012; Seward et al., 2003; van de Wiel et al., 2018), which could impact pharmacotherapy. The current lack of a high-resolution OSTα/β structure has prevented detailed structure/function studies of this transporter and identification of potential drug substrates and/or inhibitors. Here, we aimed to identify specific OSTα residues that are important for OSTα/β-mediated bile acid transport through computational modeling and site-directed mutagenesis, followed by analysis of protein expression, localization, and function. Given the bidirectionality of OSTα/β transport, both [^{3}H]-TCA uptake and efflux were evaluated for each OSTα/β mutant.

Given that OSTα is believed to be the substrate-binding subunit (Seward et al., 2003), only OSTα was selected for the final molecular dynamic simulation to test stability of the modeled transmembrane helices and to determine whether the TCA ligand remained within the cavity under the conditions tested. While we did consider modeling interactions between OSTα and OSTβ based on the LAT1-4F2hc heterodimer, the homology was insufficient and its physiological function too distant to consider it within the same genetic subfamily; therefore, assessing the location of interaction derived from this complex seemed unlikely. Of the mutants informed by evolutionary conservation and topology prediction tools, both Gln269 mutants Q269E and Q269K displayed reduced uptake, but the Q269K mutant also demonstrated reduced % efflux. Based on the molecular model and docking, Gln269 faces the OSTα cavity towards the TCA substrate. The change to glutamate adds a negative charge but this amino acid is similar in

Molecular Pharmacology Fast Forward. Published on October 1, 2021 as DOI: 10.1124/molpharm.121.000345
This article has not been copyedited and formatted. The final version may differ from this version.

size to glutamine, while lysine adds a positive charge and is considerably larger in volume than both glutamate and glutamine. Therefore, it is reasonable to assume that changes in charge and/or volume of this residue impact electrostatic interactions with the negatively charged TCA and its recognition and/or transport, with Q269K showing more notable effects as expected.

It is currently unknown whether bidirectional transport mediated by OSTα/β is truly symmetric or asymmetric (Beaudoin et al., 2020a). While some mutants (i.e., T229S, Q269E, E305A) appear to have a different impact on [^{3}H]-TCA uptake compared with efflux, it is unclear whether this is due to inherent asymmetric OSTα/β transport of the substrate, or whether differences in the experimental setup between uptake and efflux studies (e.g., efflux studies required an additional preloading phase) could have contributed, in part, to these observed differences. The S228K mutant (but not S228T) showed decreased uptake and % efflux relative to OSTα/β WT. Given the location of the Ser228 residue at the interface between two helices, it is understandable that the small difference between neutral, uncharged hydroxyl-containing serine and threonine residues may not create as drastic a change as the introduction of a basic and larger lysine that might disrupt helix-helix interactions. A relatively conservative mutation at the OSTα 229 position (T229S) resulted in reduced uptake but had no effect on efflux. This change could not be easily explained by the model as the residue did not face the OSTα cavity. Lastly, the only lysine-substituted mutant (Q260K) that did not show any differences from OSTα/β WT in uptake or % efflux could be rationalized by the outward projection of this residue, away from the TCA substrate, in the model. Two mutants (T229K, Q260E) were not investigated due to failed cell line development (*data not shown*). As anticipated, lysine substitution generally had a greater impact on OSTα/β-mediated bile acid transport than a more conservative change of the same residue (Bordo and Argos, 1991; Wong and Kwon, 2015). Of

Molecular Pharmacology Fast Forward. Published on October 1, 2021 as DOI: 10.1124/molpharm.121.000345
This article has not been copyedited and formatted. The final version may differ from this version.

the four OSTα residues selected for alanine scanning mutagenesis by using homology models, only the E305A mutant showed alterations in [^{3}H]-TCA transport, despite orientation of all these amino acids towards the docked TCA substrate. Since OsSweet residues that correspond to OSTα Phe122 and Asn298 form a contact with the sugar substrate (Tao et al., 2015), it was somewhat unexpected that F122A and N298A mutations had no effect on [^{3}H]-TCA transport. Substitutions other than alanine might be more effective, or alternatively, an improved alignment method might indicate neighboring residues that would be more important. Nonetheless, the E305A mutation reduced [^{3}H]-TCA % efflux. This residue faces the cavity orienting towards TCA's D-ring and side chain (Fig. 3; Supplemental Fig. 2, Data Supplement 2 and 3). Incidentally, the corresponding residue in OsSweet contributes to the intracellular gate that regulates substrate access to the cavity (Tao et al., 2015), suggesting that the OSTα residue Glu305 may play a role in efflux of bile acids.

Alterations in OSTα and/or OSTβ membrane localization (Supplemental Fig. 5; Supplemental Table 2) and/or reductions in protein levels (Supplemental Fig. 4) were observed for each mutant. However, several of these mutants (C103A, F122A, S228T, Q260K, N298A) showed similar uptake and % efflux data relative to OSTα/β WT (Fig. 4). There are two possible explanations for these observations: First, these mutations in OSTα actually increase the efficiency of OSTα/β-mediated transport. This phenomenon has been documented in site-directed mutagenesis studies of plant transporters (Fontenot et al., 2015; Wang et al., 2017). Additionally, site-directed mutagenesis of a highly conserved residue in human glutathione S-transferase resulted in increased substrate affinity and metabolic activity of the enzyme (Kalita et al., 2020). Second, OSTα/β is a high capacity transporter that is non-saturable at 1 mM [^{3}H]-TCA (Suga et al., 2019), and limited only by the amount of protein available for transport

Molecular Pharmacology Fast Forward. Published on October 1, 2021 as DOI: 10.1124/molpharm.121.000345
This article has not been copyedited and formatted. The final version may differ from this version.

(Malinen et al., 2018). In the present study, the level of OSTα/β protein available for efficient [^{3}H]-TCA transport was likely more than sufficient for the majority of mutant cell lines at the studied concentration (5 μM). The Q269K mutant cell line is the most obvious exception, since this mutant exhibited the lowest (i.e., negligible) expression of mature OSTα and OSTβ among all mutant cell lines investigated by Western blot, and had the most prominent effect on transport (both uptake and efflux). The substantial decreases in OSTα/β protein expression but modest reductions in [^{3}H]-TCA transport by mutants S228K, T229S, Q269E and E305A suggest that the observed differences in OSTα/β-mediated transport are driven only partially by altered plasma membrane localization, misfolding, or reduced expression. Nevertheless, future studies are needed to investigate the underlying mechanism(s) (e.g., intrinsic activity, protein expression) of altered [^{3}H]-TCA transport.

In the present study, the uptake and efflux of [^{3}H]-TCA by OSTα/β WT and mutants were investigated only at a single time point and concentration. Kinetic parameters V_{max} and K_m were not assessed here because OSTα/β was not saturable at the highest soluble concentration (1 mM) of [^{3}H]-TCA (Malinen et al., 2018). Therefore, a single time point (*i.e.*, 30-sec uptake, 5-min efflux) and concentration (5 μM) for each assay were selected based on previously published data as described in the Methods section. Another limitation is the adjustment of transport function data using total cellular protein instead of total membrane-associated OSTα/β protein. Currently available membrane extraction methods also capture intracellular organelle-bound proteins (Bunger et al., 2009). However, the non-functional, immature OSTα associates with intracellular organelles (Dawson et al., 2005; Soroka et al., 2008); therefore, the membrane-bound fraction would also likely capture this nonfunctional transport protein. Additionally, the proper stoichiometry of OSTα/β has yet to be definitively determined (Beaudoin et al., 2020a).

Molecular Pharmacology Fast Forward. Published on October 1, 2021 as DOI: 10.1124/molpharm.121.000345
This article has not been copyedited and formatted. The final version may differ from this version.

Additional studies would be needed to investigate whether the reduction in uptake and/or % efflux observed for select mutants (S228K, T229S, Q269E, Q269K, E305A) was due to decreased OSTα/β protein levels and/or plasma membrane localization rather than alterations in intrinsic transport activity.

While previous studies have investigated naturally occurring OSTα/β mutations (Schwarz, 2012; Sultan et al., 2018), the present study is the first to investigate synthetic OSTα mutations informed by computational modeling to evaluate OSTα/β protein structure/function. However, all models with low similarity between the template and the target sequences are sensitive to changes in alignment of the transmembrane helices. A difference of one amino acid in helix assignments may shift one residue that points to the cavity to face the neighboring helix or even the surrounding lipid membrane, thereby altering the quaternary structure of the protein. In summary, our data provide insight that can be utilized to inform future investigations of OSTα/β protein structure. With the novel identification of four OSTα residues (Ser228, Thr229, Gln269, Glu305) impacting bile acid transport, molecular modeling approaches can be refined for this protein to facilitate identification of additional endogenous and exogenous substrates and/or inhibitors of OSTα/β.

Molecular Pharmacology Fast Forward. Published on October 1, 2021 as DOI: 10.1124/molpharm.121.000345
This article has not been copyedited and formatted. The final version may differ from this version.

Acknowledgements

The authors would like to acknowledge Dr. Matthew Welch for assistance with evolutionary conservation analysis and topology prediction, Dr. Matthew Loop for consultation on statistical data analysis, Dr. Aaron Devanathan for assistance in creating Fig. 4, Dr. Jacqueline B. Tiley for assistance in cell culture maintenance and storage, and Arunangshu Chakrabarty and Lilly Wong for assistance with mutagenesis procedures. Dr. Tuomo Laitinen would like to acknowledge the CSC-IT Center for Science Ltd. (Finland) for the allocation of computational resources. The Visual Abstract was created with BioRender.com and Protter version 1.0. This work was presented at the 2020 American Society of Clinical Pharmacology and Therapeutics (ASCPT) Annual Meeting and International Transporter Consortium ASCPT Post-Conference Workshop 4, and published as an abstract in Clinical Pharmacology and Therapeutics 109(S1):S6 (PI-006), 2021.

Molecular Pharmacology Fast Forward. Published on October 1, 2021 as DOI: 10.1124/molpharm.121.000345
This article has not been copyedited and formatted. The final version may differ from this version.

Authorship Contributions

Participated in research design: Murphy, Beaudoin, Malinen, Swaan, Honkakoski, Brouwer.

Conducted experiments: Murphy, Beaudoin, Laitinen, Sjöstedt, Malinen, Ho, Honkakoski.

Contributed new reagents or analytic tools: Laitinen, Malinen.

Performed data analysis: Murphy, Beaudoin, Laitinen, Honkakoski, Brouwer.

Wrote or contributed to the writing of the manuscript: Murphy, Beaudoin, Laitinen, Sjöstedt, Swaan, Honkakoski, Brouwer.

Molecular Pharmacology Fast Forward. Published on October 1, 2021 as DOI: 10.1124/molpharm.121.000345
This article has not been copyedited and formatted. The final version may differ from this version.

References

Bates D, Maechler M, Bolker B and Walker S (2015) Fitting Linear Mixed-Effects Models using lme4. *J Stat Softw* **67**: 1-48.

Ballatori N (2005) Biology of a novel organic solute and steroid transporter, OSTalpha OSTbeta. *Exp Biol Med (Maywood)* **230**: 689-698.

Beaudoin JJ, Brouwer KLR and Malinen MM (2020a) Novel insights into the organic solute transporter alpha/beta, OSTalpha/beta: From the bench to the bedside. *Pharmacol Ther* **211**: 107542.

Beaudoin JJ, Bezencon J, Sjostedt N, Fallon JK and Brouwer KLR (2020b) Role of organic solute transporter alpha/beta in hepatotoxic bile acid transport and drug interactions. *Toxicol Sci* **176**: 34-45.

Bordo D and Argos P (1991) Suggestions for "safe" residue substitutions in site-directed mutagenesis. *J Mol Biol* **217**: 721-729.

Boyer JL, Trauner M, Mennone A, Soroka CJ, Cai SY, Moustafa T, Zollner G, Lee JY and Ballatori N (2006) Upregulation of a basolateral FXR-dependent bile acid efflux transporter OSTalpha-OSTbeta in cholestasis in humans and rodents. *Am J Physiol Gastrointest Liver Physiol* **290**: G1124-1130.

Bunger S, Roblick UJ and Habermann JK (2009) Comparison of five commercial extraction kits for subsequent membrane protein profiling. *Cytotechnology* **61**: 153-159.

Chai J, Feng X, Zhang L, Chen S, Cheng Y, He X, Yang Y, He Y, Wang H, Wang R and Chen W (2015) Hepatic expression of detoxification enzymes is decreased in human obstructive cholestasis due to gallstone biliary obstruction. *PLoS One* **10**: e0120055.

Cserzö M, Wallin E, Simon I, von Heijne G and Elofsson A (1997) Prediction of transmembrane

alpha-helices in prokaryotic membrane proteins: the dense alignment surface method. *Protein Eng* **10**: 673-676.

Dawson PA, Hubbert M, Haywood J, Craddock AL, Zerangue N, Christian WV and Ballatori N (2005) The heteromeric organic solute transporter alpha-beta, Ostalpha-Ostbeta, is an ileal basolateral bile acid transporter. *J Biol Chem* **280**: 6960-6968.

Dawson PA, Hubbert ML and Rao A (2010) Getting the mOST from OST: role of organic solute transporter, OSTalpha-OSTbeta, in bile acid and steroid metabolism. *Biochim Biophys Acta* **1801**: 994-1004.

Di Ciaula A, Garruti G, Lunardi Baccetto R, Molina-Molina E, Bonfrate L, Wang DQ and Portincasa P (2017) Bile acid physiology. *Ann Hepatol* **16**: s4-s14.

Dobson L, Reményi I and Tusnády GE (2015) CCTOP: a consensus constrained TOPology prediction web server. *Nucleic Acids Res* **43**: W408-412.

Fontenot EB, Ditusa SF, Kato N, Olivier DM, Dale R, Lin WY, Chiou TJ, Macnaughtan MA and Smith AP (2015) Increased phosphate transport of arabidopsis thaliana pht1;1 by site-directed mutagenesis of tyrosine 312 may be attributed to the disruption of homomeric interactions. *Plant Cell Environ* **38**: 2012-2022.

Gao E, Cheema H, Waheed N, Mushtaq I, Erden N, Nelson-Williams C, Jain D, Soroka CJ, Boyer JL, Khalil Y, Clayton PT, Mistry PK, Lifton RP and Vilarinho S (2019) OSTalpha deficiency: a disorder with cholestasis, liver fibrosis and congenital diarrhea. *Hepatology* **71**: 1879-1882.

Goodrich B, Gabry J, Ali I and Brilleman S (2020) rstanarm: Bayesian applied regression modeling via Stan. R package version 2.21.1. URL: http://mc-stan.org/rstanarm

Gruetz M, Sticht H, Glaeser H, Fromm MF, König J (2016) Analysis of amino acid residues in

the predicted transmembrane pore influencing transport kinetics of the hepatic drug transporter organic anion transporting polypeptide 1B1 (OATP1B1). *Biochim Biophys Acta* **1858**: 2894-2902.

Guo C, LaCerte C, Edwards JE, Brouwer KR and Brouwer KLR (2018) Farnesoid X receptor agonists obeticholic acid and chenodeoxycholic acid increase bile acid efflux in sandwich-cultured human hepatocytes: functional evidence and mechanisms. *J Pharmacol Exp Ther* **365**: 413-421.

Hirokawa T, Boon-Chieng S and Mitaku S (1998) SOSUI: classification and secondary structure prediction system for membrane proteins. *Bioinformatics* **14**: 378-379.

Ikeda M, Arai M, Okuno T and Shimizu T (2003) TMPDB: a database of experimentally-characterized transmembrane topologies. *Nucleic Acids Res* **31**: 406-409.

Kalita J, Shukla H and Tripathi T (2020) Engineering glutathione S-transferase with a point mutation at conserved F136 residue increases the xenobiotic-metabolizing activity. *Int J Biol Macromol* **163**: 1117-1126.

Krogh A, Larsson B, von Heijne G and Sonnhammer EL (2001) Predicting transmembrane protein topology with a hidden markov model: application to complete genomes. *J Mol Biol* **305**: 567-580.

Larkin MA, Blackshields G, Brown NP, Chenna R, McGettigan PA, McWilliam H, Valentin F, Wallace IM, Wilm A, Lopez R, Thompson JD, Gibson TJ and Higgins DG (2007) Clustal W and Clustal X version 2.0. *Bioinformatics* **23**: 2947-2948.

Malinen MM, Ali I, Bezencon J, Beaudoin JJ and Brouwer KLR (2018) Organic solute

transporter OSTalpha/beta is overexpressed in nonalcoholic steatohepatitis and modulated by drugs associated with liver injury. *Am J Physiol Gastrointest Liver Physiol* **314**: G597-G609.

Malinen MM, Kauttonen A, Beaudoin JJ, Sjöstedt N, Honkakoski P and Brouwer KLR (2019) Novel in vitro method reveals drugs that inhibit organic solute transporter alpha/beta (OSTalpha/beta). *Mol Pharm* **16**: 238-246.

Morrison KL and Weiss GA (2001) Combinatorial alanine-scanning. *Curr Opin Chem Biol* **5**: 302-307.

Notredame C, Higgins DG and Heringa J (2000) T-Coffee: a novel method for fast and accurate multiple sequence alignment. *J Mol Biol* **302**: 205-217.

Nugent T and Jones DT (2012) Detecting pore-lining regions in transmembrane protein sequences. *BMC Bioinformatics* **13**: 169.

Omasits U, Ahrens CH, Muller S and Wollscheid B (2014) Protter: interactive protein feature visualization and integration with experimental proteomic data. *Bioinformatics* **30**: 884-886.

Pasquier C, Promponas VJ, Palaios GA, Hamodrakas JS and Hamodrakas SJ (1999) A novel method for predicting transmembrane segments in proteins based on a statistical analysis of the SwissProt database: the PRED-TMR algorithm. *Protein Eng* **12**: 381-385.

Pei J, Kim BH and Grishin NV (2008) PROMALS3D: a tool for multiple protein sequence and structure alignments. *Nucleic Acids Res* **36**: 2295-2300.

R Core Team (2020) R: A language and environment for statistical computing. R Foundation for Statistical Computing, Vienna, Austria. URL: http://www.R-project.org/

Scalise M, Pochini L, Console L, Pappacoda G, Pingitore P, Hedfalk K and Indiveri C (2018)

Cys site-directed mutagenesis of the human SLC1A5 (ASCT2) transporter: structure/function relationships and crucial role of Cys467 for redox sensing and glutamine transport. *Int J Mol Sci* **19**: 648.

Schlessinger A, Welch MA, van Vlijmen H, Korzekwa K, Swaan PW and Matsson P (2018) Molecular modeling of drug-transporter interactions-an international transporter consortium perspective. *Clin Pharmacol Ther* **104**: 818-835.

Schneider CA, Rasband WS and Eliceiri KW (2012) NIH Image to ImageJ: 25 years of image analysis. *Nat Methods* **9**: 671-675.

Schwarz UI (2012) The bile acid transporter organic solute transporter (OST) alpha-beta is also an intestinal drug transporter, in *Intestinal and hepatic drug transporters and their role in the disposition of lipid-lowering drugs* (Kim RB ed) pp 81-112, The University of Western Ontario, Electronic Thesis and Dissertation Repository.

Seward DJ, Koh AS, Boyer JL and Ballatori N (2003) Functional complementation between a novel mammalian polygenic transport complex and an evolutionarily ancient organic solute transporter, OSTalpha-OSTbeta. *J Biol Chem* **278**: 27473-27482.

Soroka CJ, Xu S, Mennone A, Lam P and Boyer JL (2008) N-Glycosylation of the alpha subunit does not influence trafficking or functional activity of the human organic solute transporter alpha/beta. *BMC Cell Biol* **9**: 57.

Suga T, Yamaguchi H, Ogura J and Mano N (2019) Characterization of conjugated and unconjugated bile acid transport via human organic solute transporter alpha/beta. *Biochim Biophys Acta Biomembr* **1861**: 1023-1029.

Sultan M, Rao A, Elpeleg O, Vaz FM, Abu-Libdeh B, Karpen SJ and Dawson PA (2018)

Organic solute transporter-beta (SLC51B) deficiency in two brothers with congenital diarrhea and features of cholestasis. *Hepatology* **68**: 590-598.

Tao Y, Cheung LS, Li S, Eom JS, Chen LQ, Xu Y, Perry K, Frommer WB and Feng L (2015) Structure of a eukaryotic SWEET transporter in a homotrimeric complex. *Nature* **527**: 259-263.

The UniProt Consortium (2021) UniProt: the universal protein knowledgebase in 2021. *Nucleic Acids Research* **49**: D480-D489.

Tsirigos KD, Peters C, Shu N, Käll L and Elofsson A (2015) The TOPCONS web server for consensus prediction of membrane protein topology and signal peptides. *Nucleic Acids Res* **43**: W401-407.

Tusnády GE and Simon I (2001) The HMMTOP transmembrane topology prediction server. *Bioinformatics* **17**: 849-850.

Uhlen M, Fagerberg L, Hallstrom BM, Lindskog C, Oksvold P, Mardinoglu A, Sivertsson A, Kampf C, Sjostedt E, Asplund A, Olsson I, Edlund K, Lundberg E, Navani S, Szigyarto CA, Odeberg J, Djureinovic D, Takanen JO, Hober S, Alm T, Edqvist PH, Berling H, Tegel H, Mulder J, Rockberg J, Nilsson P, Schwenk JM, Hamsten M, von Feilitzen K, Forsberg M, Persson L, Johansson F, Zwahlen M, von Heijne G, Nielsen J and Ponten F (2015) Proteomics. Tissue-based map of the human proteome. *Science* **347**: 1260419.

van de Wiel SMW, de Waart DR, Oude Elferink RPJ, van de Graaf SFJ (2017) Intestinal farnesoid X receptor activation by pharmacologic inhibition of the organic solute transporter α-β. *Cell Mol Gastroenterol Hepatol* **5**: 223-237.

Wang C, Li Y, Qiu C, Wang S, Ma J, Shen Y, Zhang Q, Du B, Ding Y and Bao X (2017)

Identification of important amino acids in Gal2p for improving the L-arabinose transport and metabolism in saccharomyces cerevisiae. *Front Microbiol* **8**: 1391.

Wang W, Seward DJ, Li L, Boyer JL and Ballatori N (2001) Expression cloning of two genes that together mediate organic solute and steroid transport in the liver of a marine vertebrate. *Proc Natl Acad Sci U S A* **98**: 9431-9436.

Wong HE and Kwon I (2015) Effects of non-natural amino acid incorporation into the enzyme core region on enzyme structure and function. *Int J Mol Sci* **16**: 22735-22753.

Zou L, Stecula A, Gupta A, Prasad B, Chien HC, Yee SW, Wang L, Unadkat JD, Stahl SH, Fenner KS and Giacomini KM (2018) Molecular mechanisms for species differences in organic anion transporter 1, OAT1: implications for renal drug toxicity. *Mol Pharmacol* **94**: 689-699.

Footnotes

This work was supported by the National Institutes of Health (NIH) National Institute of Diabetes and Digestive and Kidney Diseases (NIDDK) [Grant F31DK120196] and the National Institute of General Medical Sciences (NIGMS) [Grant R35GM122576]. Dr. Peter Swaan received funding from NIH NIDDK [Grant R01DK61425]. Dr. Paavo Honkakoski received partial research support from the Academy of Finland [Grant 332660], the University of Eastern Finland, and the Nannerl O. Keohane Distinguished Visiting Professorship from UNC-Chapel Hill and Duke University. Dr. Tuomo Laitinen received funding from Biocenter Finland/Drug Discovery and Chemical Biology Consortium (DDCB). Dr. Melina M. Malinen received salary support from the European Union's Horizon 2020 Research and Innovation program under the Marie Skłodowska-Curie grant agreement number 799510. Dr. Noora Sjöstedt received salary support from the Sigrid Jusélius Foundation.

Conflicts of Interest

The authors declare no conflicts of interest.

Molecular Pharmacology Fast Forward. Published on October 1, 2021 as DOI: 10.1124/molpharm.121.000345
This article has not been copyedited and formatted. The final version may differ from this version.

Figure Legends

Fig. 1. Flow chart of OSTα/β mutagenesis and evaluation. Evolutionary conservation and topology prediction tools were used to identify residues for mutagenesis resulting in the following OSTα mutants: S228K, S228T, T229S, Q260K, Q269E, and Q269K. Homology models were used to identify additional OSTα residues for alanine scanning mutagenesis: C103A, F122A, N298A, and E305A. Following site-directed mutagenesis, stable Flp-In™ 293 cell lines were established for Mock, OSTα/β wild-type, and OSTα/β mutants. OSTα/β-mediated bile acid uptake and efflux, protein localization and expression were evaluated for each stable cell line. Alanine (Ala; A); Asparagine (Asn; N); Cystine (Cys; C); Glutamate (Glu; E); Glutamine (Gln; Q); Lysine (Lys; K); Phenylalanine (Phe; F); Serine (Ser; S); Threonine (Thr; T)

Fig. 2. Predicted OSTα transmembrane domains and amino acid residues selected for site-directed mutagenesis. OSTα is composed of 340 amino acids, with seven predicted transmembrane domains (The UniProt Consortium, 2021). All amino acid residues selected for mutagenesis (see Fig. 1) are highlighted in red. Every 10th amino acid residue is numbered accordingly. Protter version 1.0 (Omasits et al., 2014) was used to create this figure.

Fig. 3. Homology model of OSTα/β with the docked taurocholate (TCA) substrate. The seven OSTα helices are shown as barrels with a color gradient from H1 (red) through H4 (purple) to H7 (blue) and the single OSTβ helix as a golden barrel. All mutated amino acids are displayed with licorice structures and single-letter codes while the TCA backbone is presented as a green ball-and-stick structure with the bile acid A-ring closest to amino acids Phe122 and Asn298. The view on the left is from the cytoplasmic side into the OSTα cavity. The side view

Molecular Pharmacology Fast Forward. Published on October 1, 2021 as DOI: 10.1124/molpharm.121.000345
This article has not been copyedited and formatted. The final version may differ from this version.

on the right shows the extracellular side at the top and cytoplasmic side at the bottom. Made using PyMOL Molecular Graphics System, Version 2.0 Schrödinger, LLC.

Fig. 4. Forest plot of OSTα/β-mediated [^{3}H]-TCA 30-sec uptake and [^{3}H]-TCA % efflux of preloaded amount for OSTα/β wild-type (WT) and OSTα/β mutant cell lines. Data points represent the ratio of the geometric mean value between OSTα/β mutant and OSTα/β WT for 30-sec uptake (dark blue) and % efflux (light blue). Error bars represent the 95% credible interval. Ratios of geometric mean values and credible intervals were calculated using a Bayesian generalized linear mixed model adjusted on experimental day for both uptake and efflux data, and group number for efflux data only since a single group was evaluated for uptake assays. Across the three uptake assays, nine independent replicates were collected, in total, for all OSTα/β mutant cell lines. Similarly, for the three efflux assays, nine independent replicates were collected for all OSTα/β mutant cell lines except S228K, S228T, Q269E, and Q269K, for which eight independent replicates were collected. *95% credible interval does not cross 1.0.

Fig. 5. Western blot and immunocytochemistry of Mock, OSTα/β wild-type (WT), and OSTα/β mutant cell lines. a) OSTα and **b)** OSTβ Western blot analysis of whole cell lysate for Mock, OSTα/β WT, and OSTα/β mutant cell lines. Protein bands for mature (likely plasma membrane-localized) and immature (likely intracellular-localized) OSTα are shown slightly above and below 38 kDa, respectively, at ~14 kDa for OSTβ, and at ~42 kDa for the β-actin loading control. Images of OSTα, OSTβ, and loading control Western blots were cropped from one membrane (see Supplemental Fig. 4 for the full, uncropped membranes). Red frames on the Western blot indicate OSTα/β WT and OSTα/β mutant cell lines that demonstrated differences in [^{3}H]-TCA 30-sec uptake and/or efflux %. Immunocytochemistry staining of nuclei using DAPI (4′,6-diamidino-2-phenylindole; blue) and **c)** OSTα (green) or **d)** OSTβ (green) for OSTα/β WT

Molecular Pharmacology Fast Forward. Published on October 1, 2021 as DOI: 10.1124/molpharm.121.000345
This article has not been copyedited and formatted. The final version may differ from this version.

and for the five OSTα/β mutant cell lines that showed differences in uptake and/or efflux. Qualitative assessment of plasma membrane localization (++; strong), (+; modest), (-; negligible) is provided next to the label for each OSTα/β mutant. All qualitative measures of localization are relative to OSTα/β WT. Images were taken using a Nikon ECLIPSE Ti2 microscope with a 60X oil immersion objective (field of view ≈ 40 μm wide).

Molecular Pharmacology Fast Forward. Published on October 1, 2021 as DOI: 10.1124/molpharm.121.000345
This article has not been copyedited and formatted. The final version may differ from this version.

Fig. 1

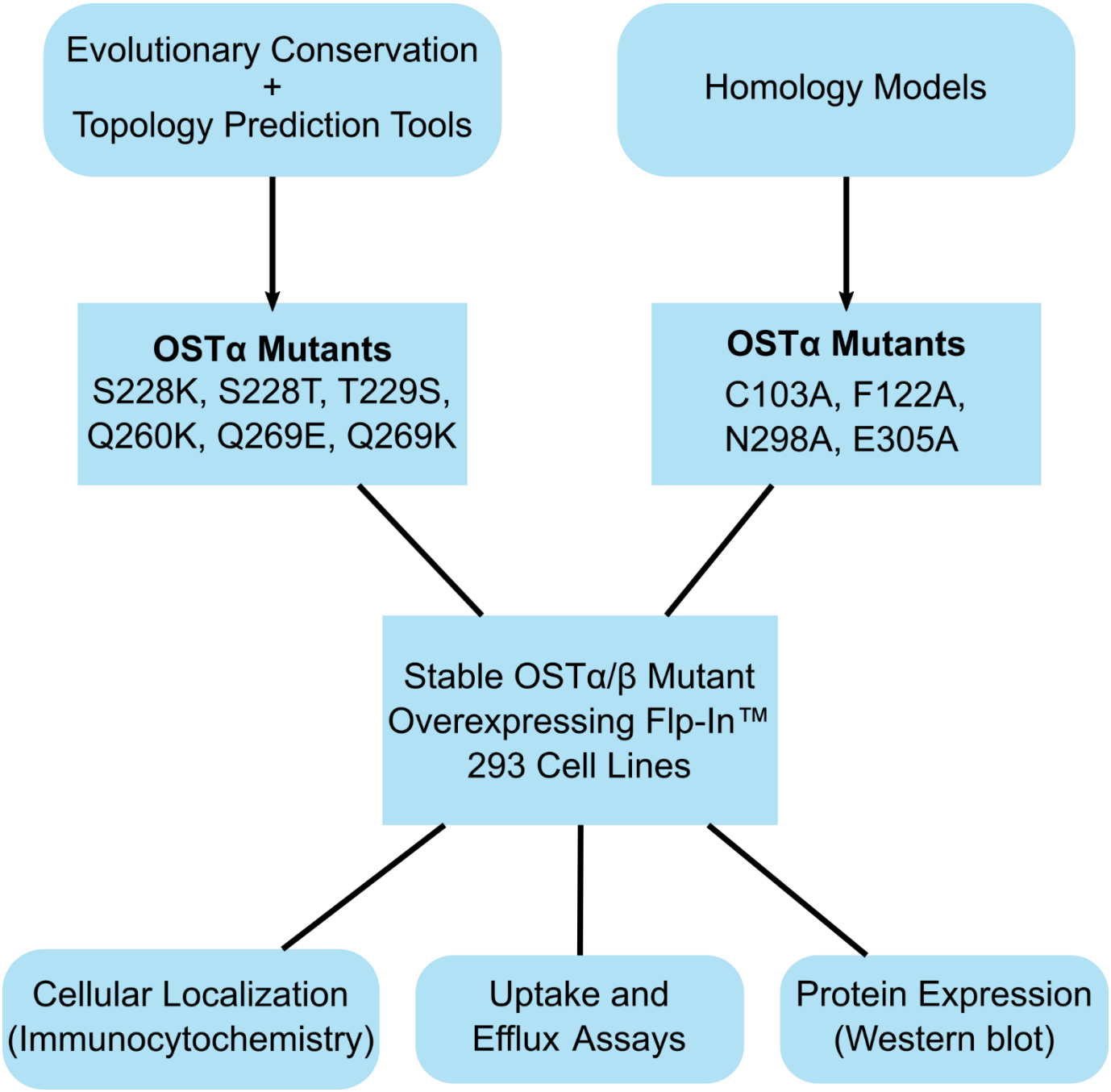

Molecular Pharmacology Fast Forward. Published on October 1, 2021 as DOI: 10.1124/molpharm.121.000345
This article has not been copyedited and formatted. The final version may differ from this version.

Fig. 2

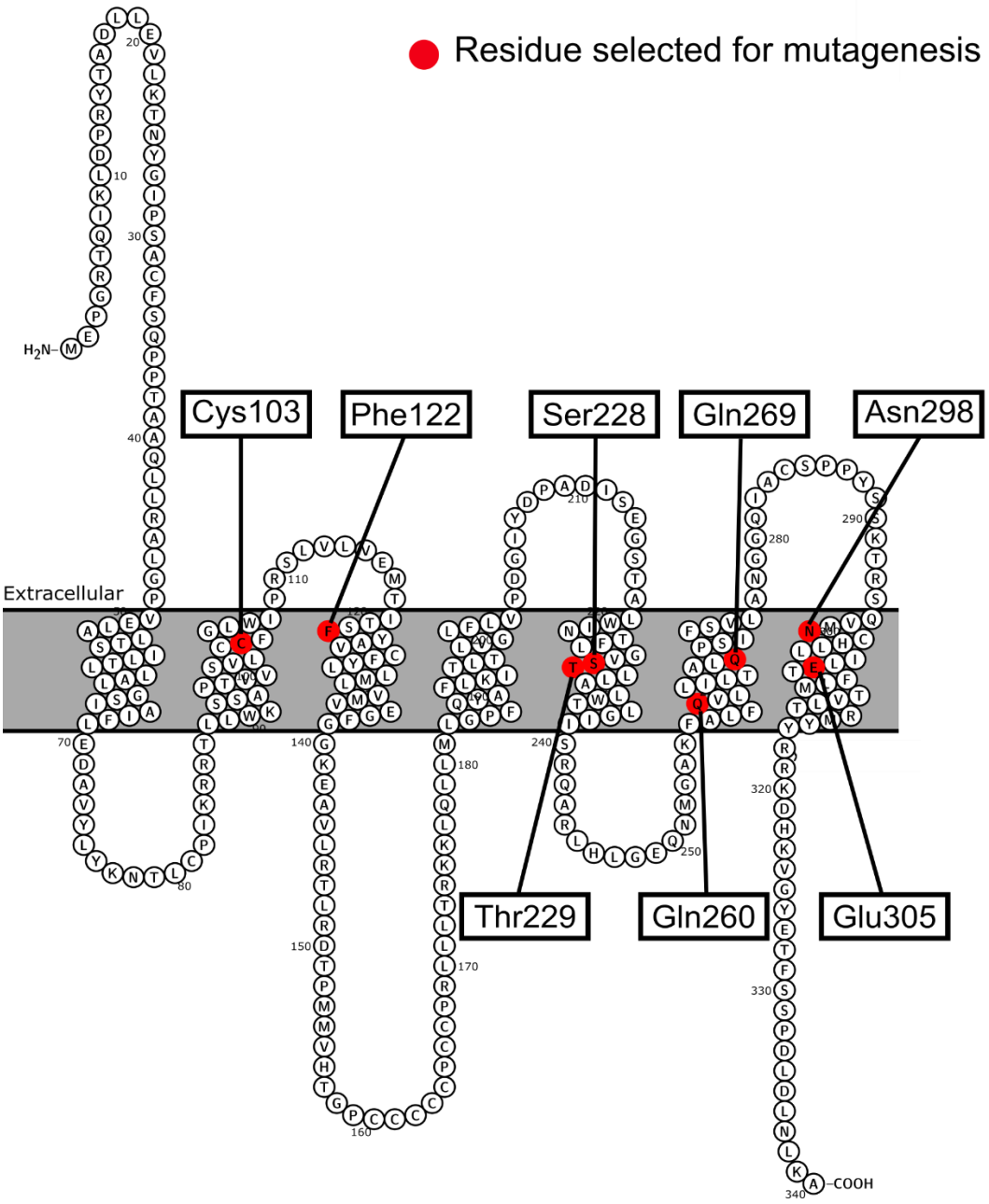

Molecular Pharmacology Fast Forward. Published on October 1, 2021 as DOI: 10.1124/molpharm.121.000345
This article has not been copyedited and formatted. The final version may differ from this version.

Fig. 3

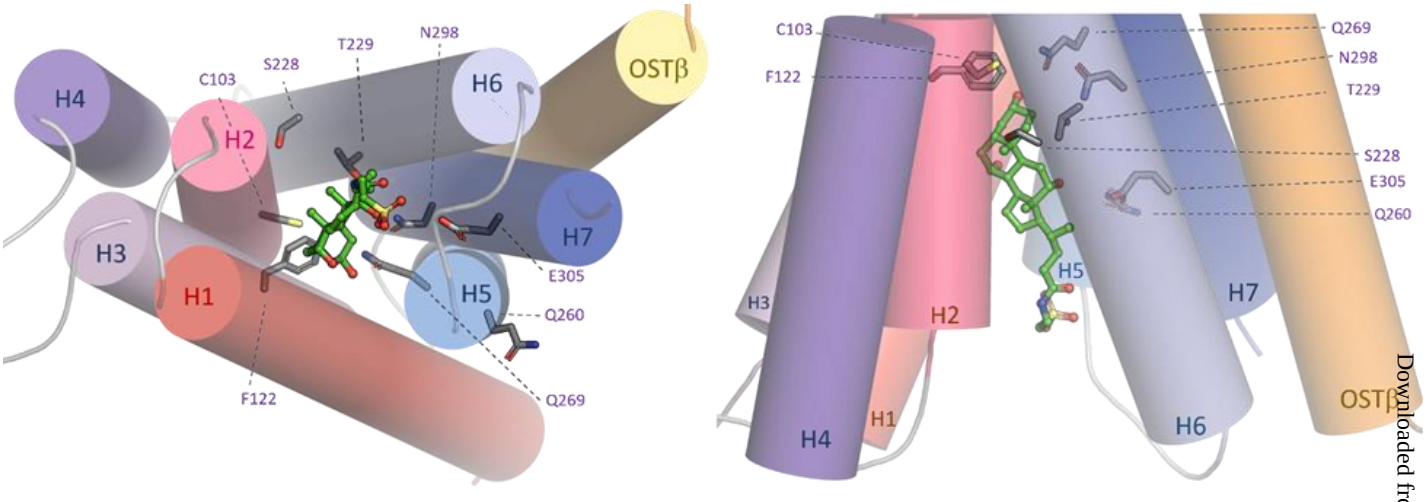

Molecular Pharmacology Fast Forward. Published on October 1, 2021 as DOI: 10.1124/molpharm.121.000345
This article has not been copyedited and formatted. The final version may differ from this version.

Fig. 4

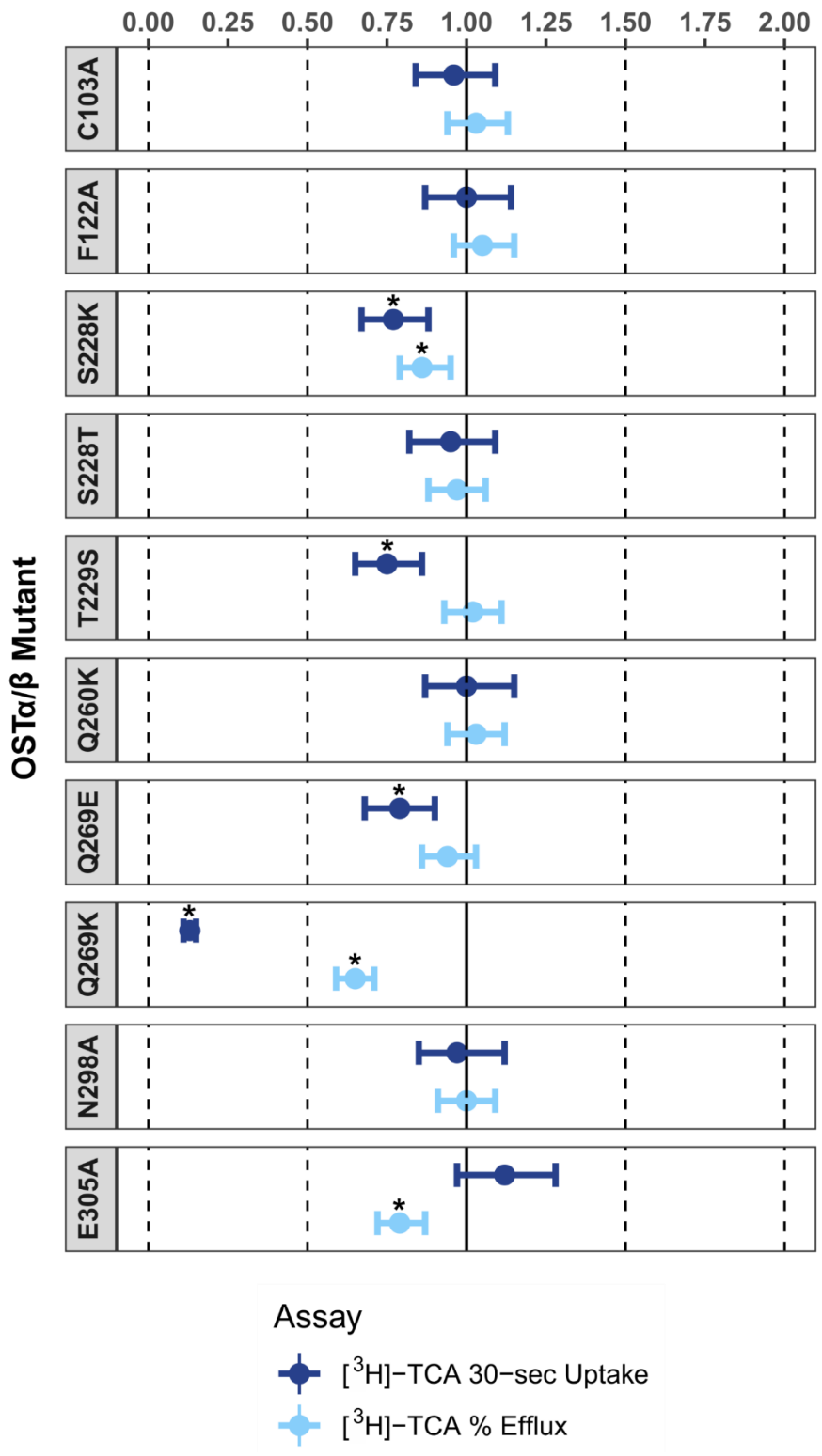

Molecular Pharmacology Fast Forward. Published on October 1, 2021 as DOI: 10.1124/molpharm.121.000345
This article has not been copyedited and formatted. The final version may differ from this version.

Fig. 5

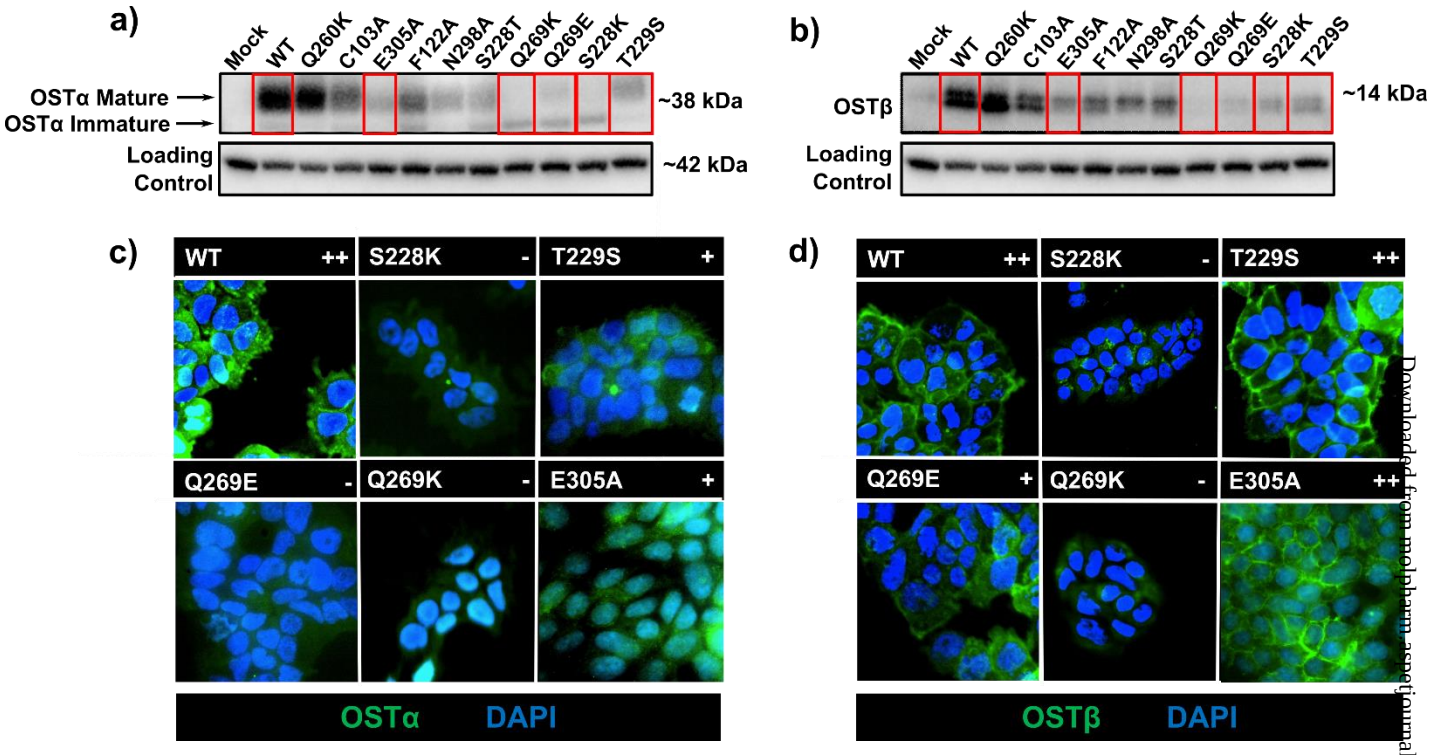

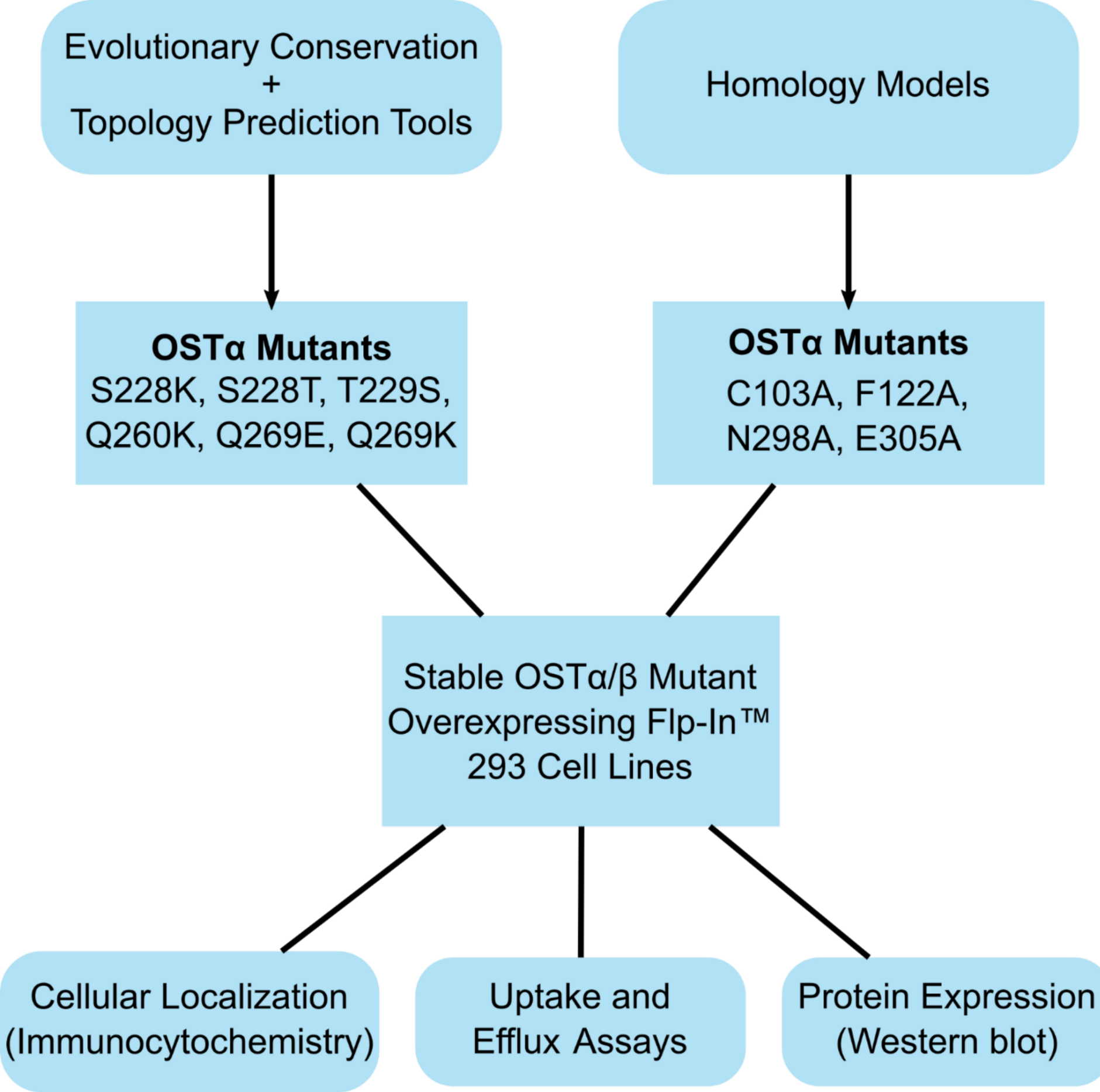
Evolutionary Conservation
+
Topology Prediction Tools
Homology Models
OSTα Mutants
S228K, S228T, T229S,
Q260K, Q269E, Q269K
OSTα Mutants
C103A, F122A,
N298A, E305A
Stable OSTα/β Mutant
Overexpressing Flp-In™
293 Cell Lines
Cellular Localization
(Immunocytochemistry)
Uptake and
Efflux Assays
Protein Expression
(Western blot)

Figure 1

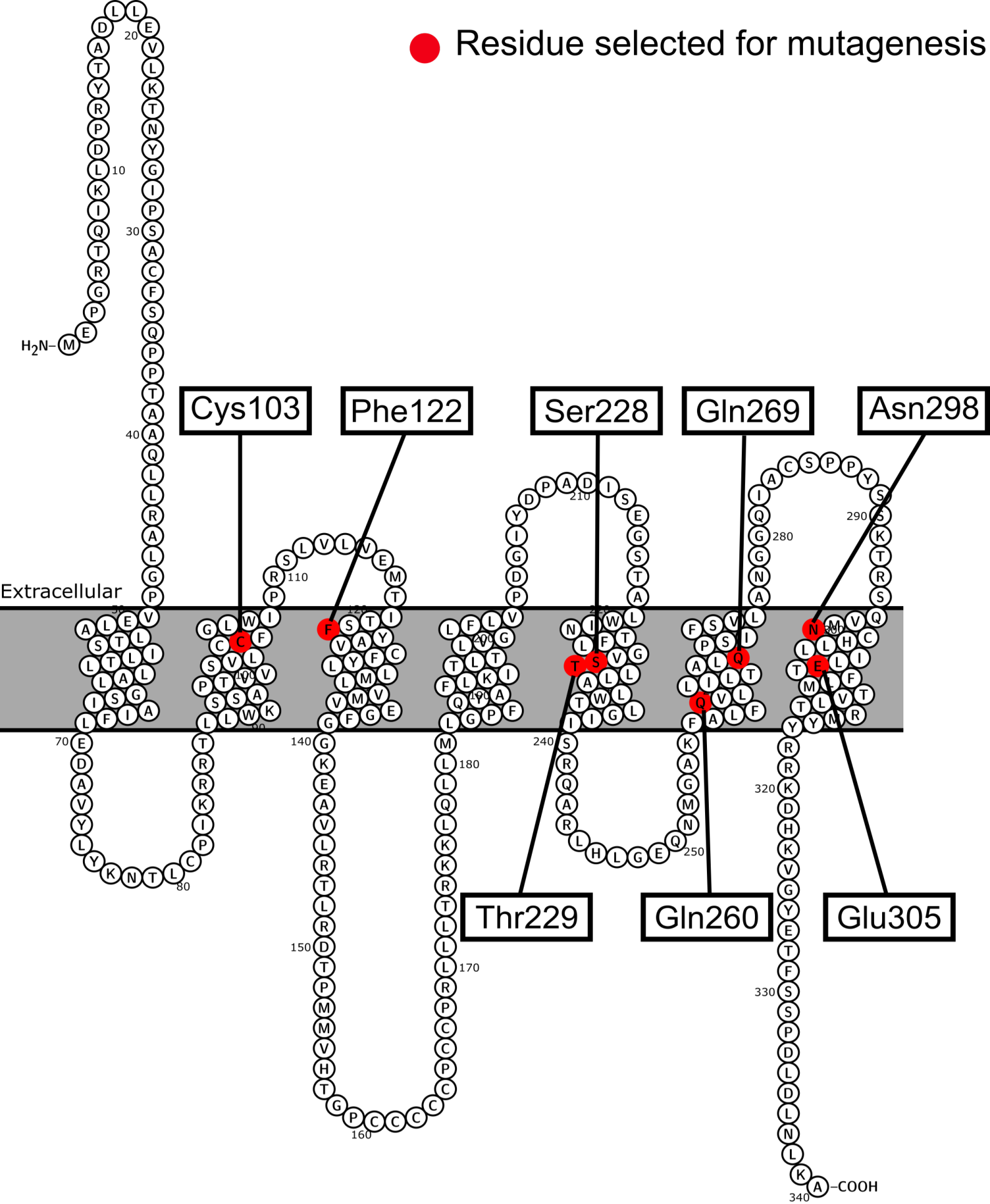
Residue selected for mutagenesis
Cys103
Phe122
Ser228
Gln269
Asn298
Thr229
Gln260
Glu305
Extracellular
H2N–
–COOH

Figure 2

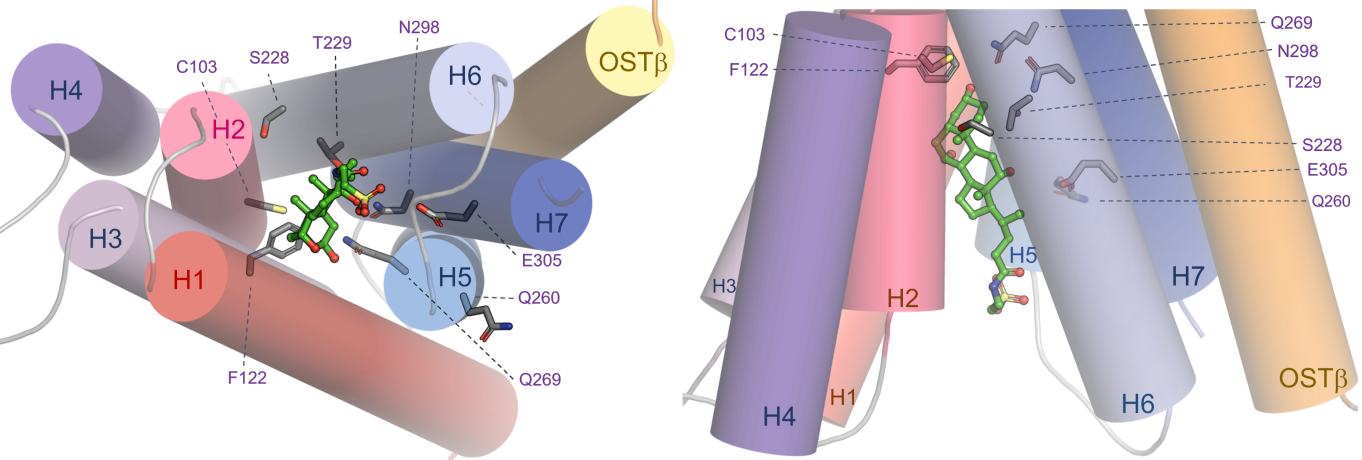
H4
C103
S228
T229
N298
H6
OSTβ
H2
H3
H7
H1
H5
E305
Q260
F122
Q269
C103
F122
Q269
N298
T229
S228
E305
Q260
H5
H3
H2
H7
H1
H4
H6
OSTβ

Figure 3

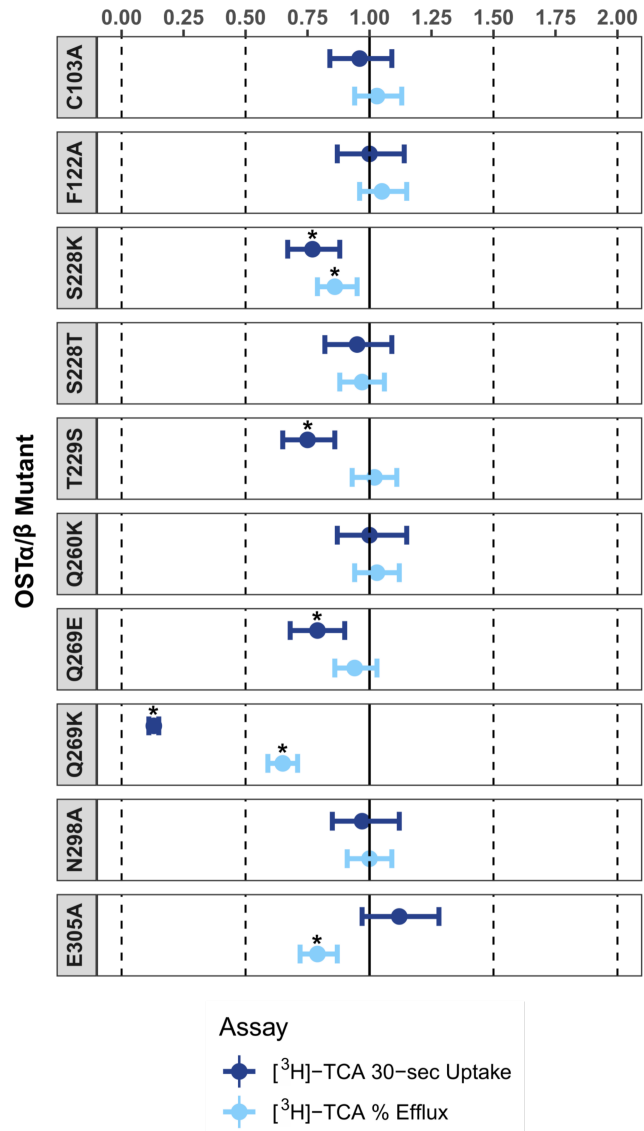
0.00
0.25
0.50
0.75
1.00
1.25
1.50
1.75
2.00
OSTα/β Mutant
C103A
F122A
S228K
S228T
T229S
Q260K
Q269E
Q269K
N298A
E305A
Assay
[3H]−TCA 30−sec Uptake
[3H]−TCA % Efflux

Figure 4

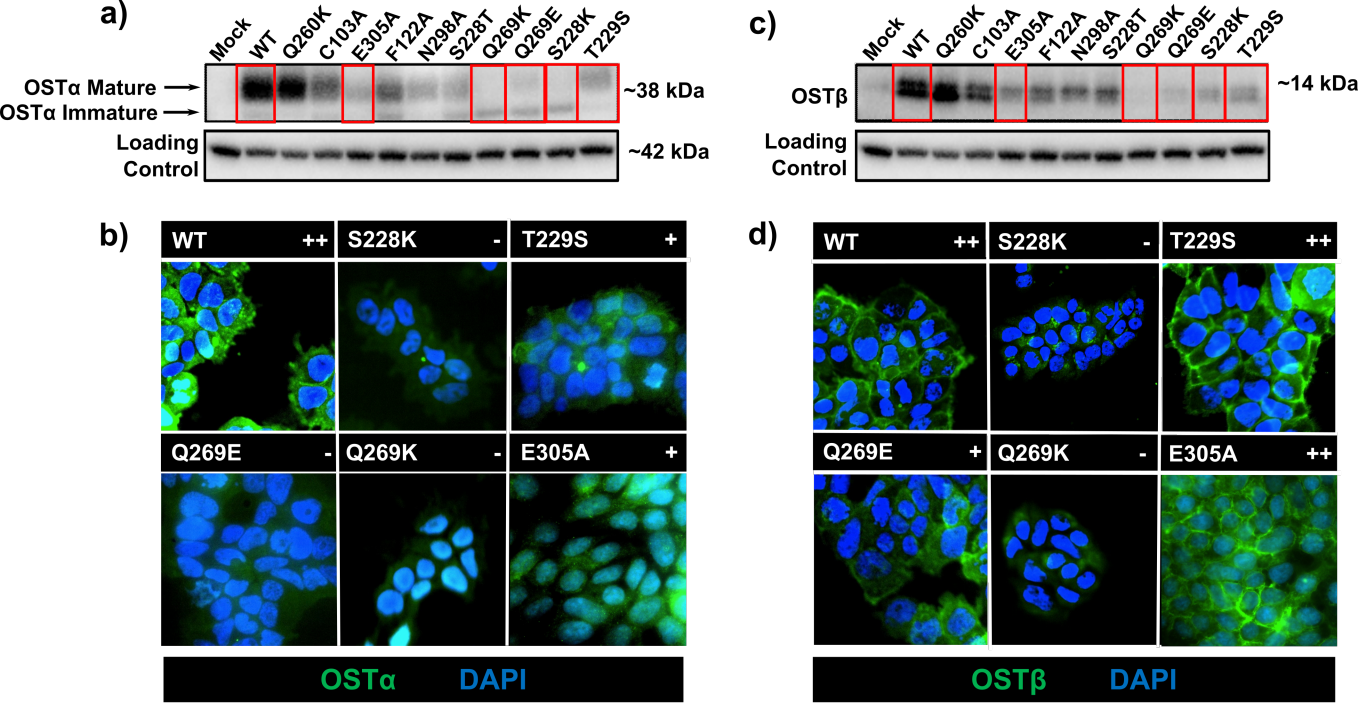
a)
Mock
WT
Q260K
C103A
E305A
F122A
N298A
S228T
Q269K
Q269E
S228K
T229S
OSTα Mature
OSTα Immature
~38 kDa
Loading Control
~42 kDa
c)
OSTβ
~14 kDa
b)
WT ++
S228K -
T229S +
Q269E -
Q269K -
E305A +
OSTα DAPI
d)
WT ++
S228K -
T229S ++
Q269E +
Q269K -
E305A ++
OSTβ DAPI

Figure 5